MONTHLY REPORT

JUNE 1975

Contract Number: NAS9-13303

QUANTITATIVE DETERMINATION OF STRATOSPHERIC AEROSOL CHARACTERISTICS

Included as supplement to this report are descriptions of our approaches in noise analysis and removal, and in relating data points to an altitude above the earth's surface. These descriptions will be updated as more is learned but otherwise will become a part of the final report. Therefore, we invite criticism by the technical monitor's office.

We are able to report encouraging results this month on the determination of attenuation coefficients as a function of altitude--the principal thrust of the investigation. The results are still tentative due to our continuing efforts to scale correctly. However, because of our progress in scaling, the limb brightness signature has been inverted and the results are indicative of results to come soon. It is clear that aerosol information is contained within the data. After treatment for noise removal and for geometric distortions inherent in the sensor data acquisition geometry and after intensity calibration, the information can be extracted. Figure 1 shows the comparison between the brightness model and the measured data after calibration and scaling. The model is based on the results reported by Elterman (1968) (referenced in a previous report). The model has been converted to that signal which would be recorded by the S192 sensor. Figure 2 shows the inversion of this measured signature as the profile of attenuation coefficients versus altitude. For comparison we include Elterman's models (1964 and 1968) in Figures 3A and 3B which show some of the same characteristics although the altitude scale is not the same. Both curves represent the attenuation coefficient's as turbidity, the ratio of aerosol coefficients to Rayleigh coefficients. It should be noted that a change in altitude scale will change the amplitudes of the profile. Further work is presently being concentrated in this area.

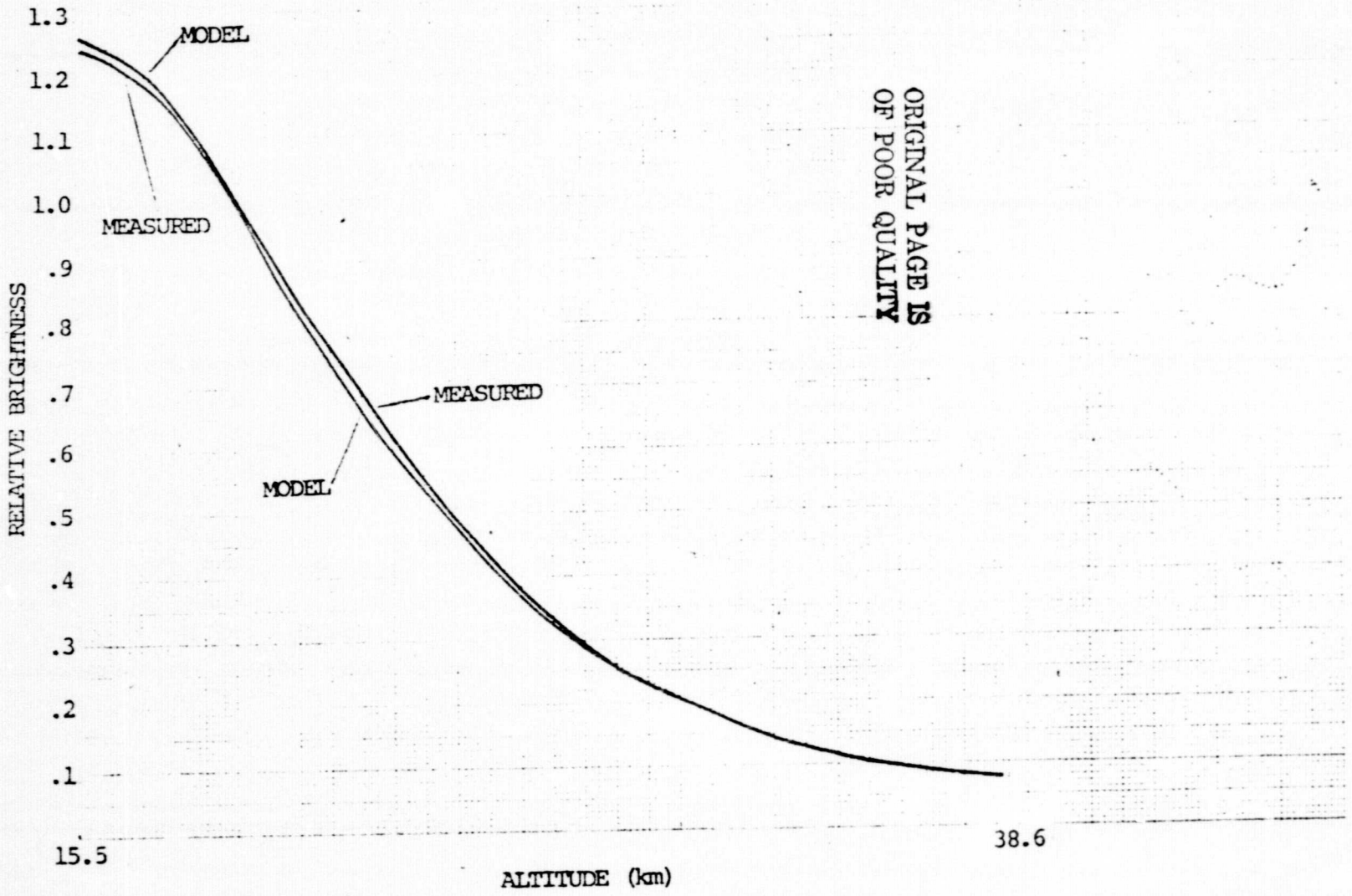

FIGURE 1

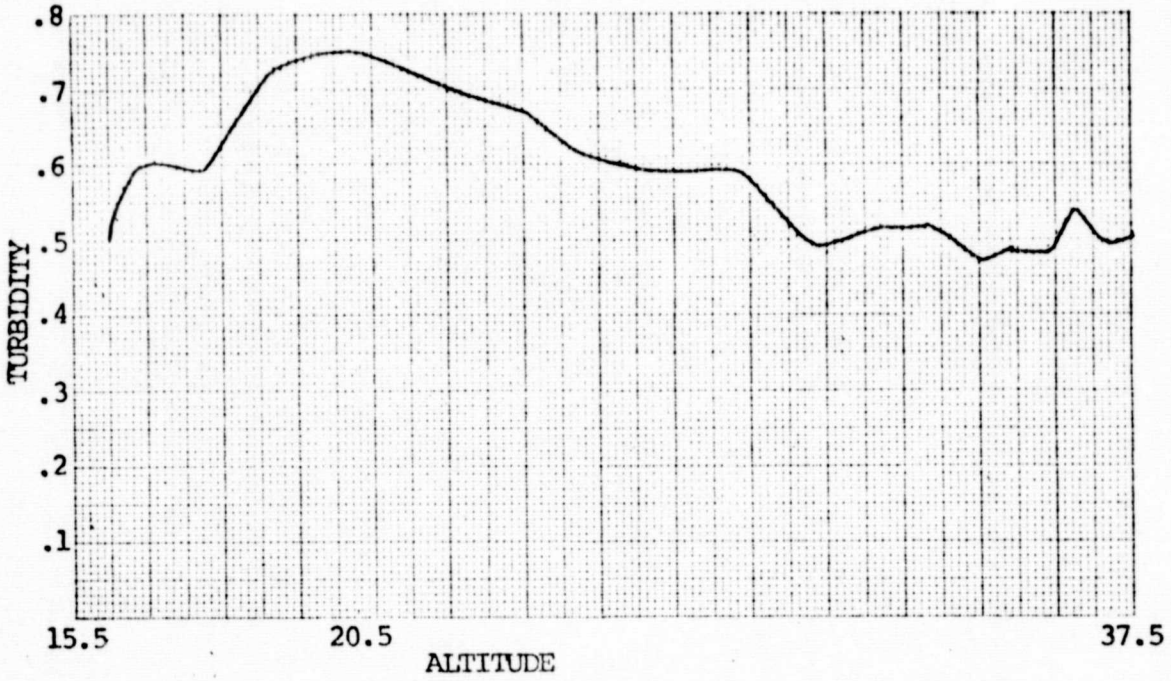

CH 22

FIGURE 2

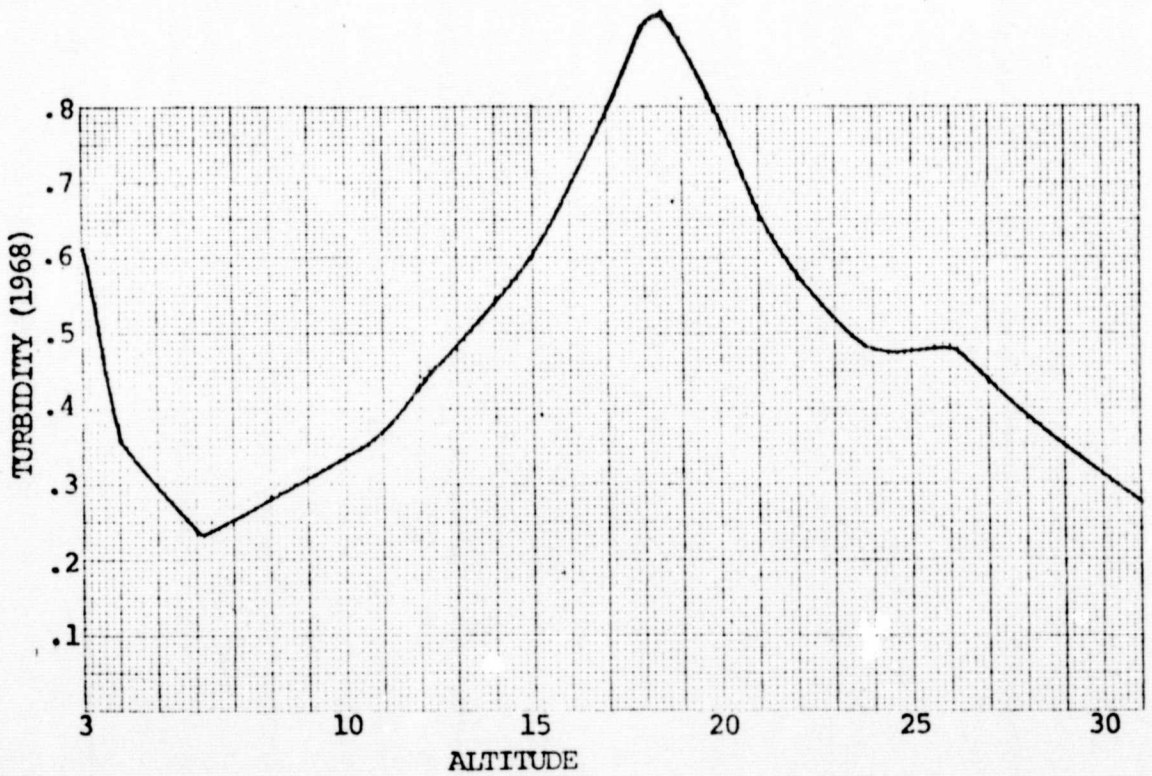

FIGURE 3B

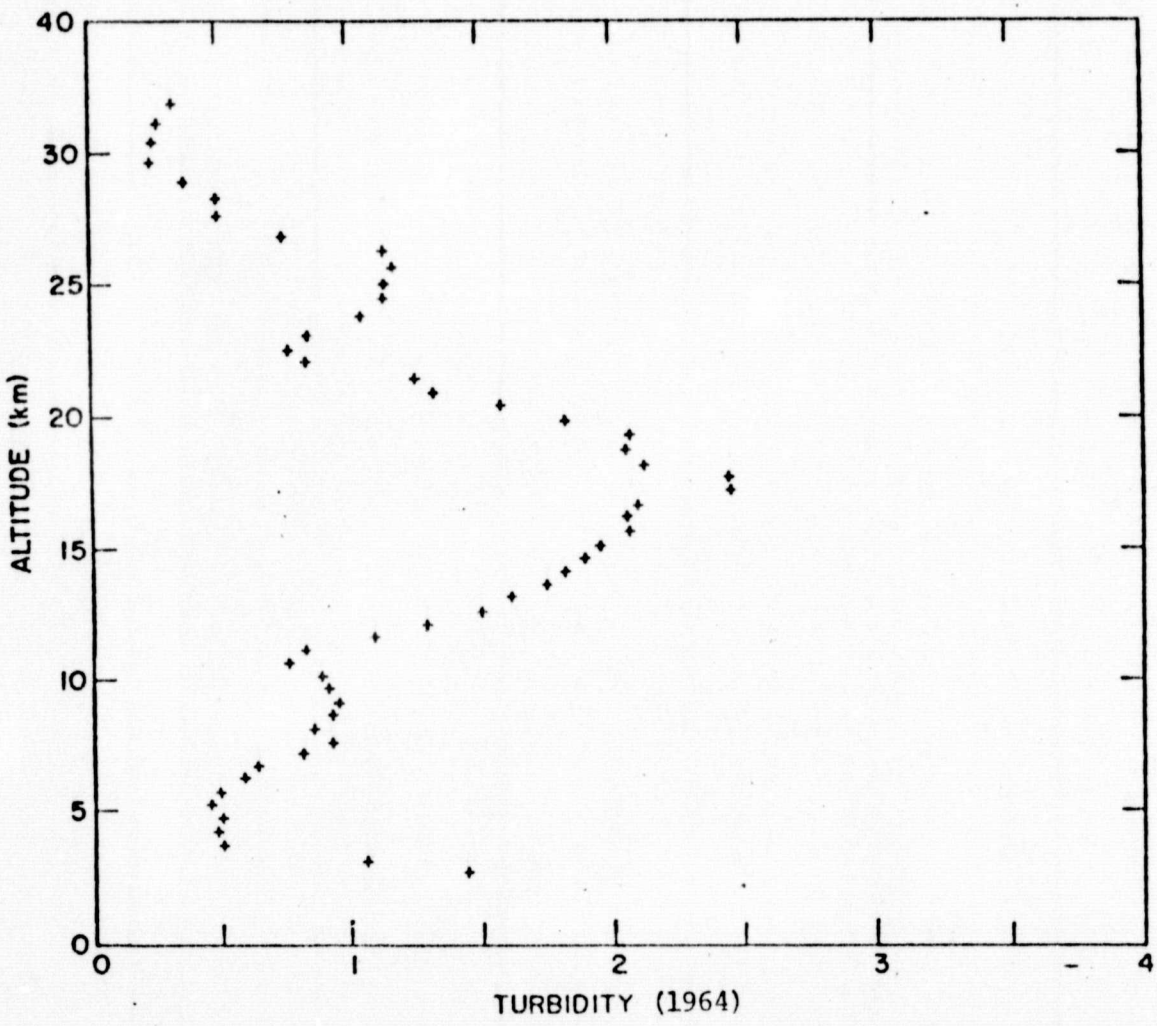

FIGURE 3.A

APPENDIX A

NOISE ANALYSIS

A. Periodic Noise

Given a reported 17 cycles/sec periodic noise and a S192 scan rate of 94 scans/sec we searched for a noise periodicity in the neighborhood of 5.5 scans/cycle. Data used in the initial analysis was from Pass 47, tape 934527, channel 18, scans 101-120.

Because of the gaussian noise we were unable to use the measured data directly. We fit the data with two exponential curves, one covering the lower altitude and the other covering the higher altitude. The two curves were smoothly joined by weighting one curve decreasingly as the other curve is weighted increasingly; e.g.,

$$\frac{.9\,P_1^1 \quad .8\,P_2^1 \quad .7\,P_3^1 \ \ldots \qquad .1\,P_1^2 \quad .2\,P_2^2 \quad .3\,P_3^2 \ \ldots}{(.9\,P_1^1 + .1\,P_1^2)(.8\,P_2^1 + .2\,P_2^2) \ \ldots\ldots}$$

The exponential curves were then used to represent the data for their respective scans.

A twenty point curve was derived by selecting a data point and plotting its value from each of twenty adjacent scans. Several curves were obtained by repeating the process for every tenth data point. To emphasize differences and to minimize effects of amplitude, the lowest value on each twenty point curve was subtracted from the respective curves. Because the magnitude of these resultant curves was constant throughout all curves (through all altitudes) it was concluded that the noise was additive.

We found that the noise from the lower altitudes was erratic. This data was not considered in the derivation of the noise periodicity. From about point 70 (assigning 1 to the first useful limb data point) the curves appear periodic, especially within points 90-130. In this region the noise is definitely periodic and all curves are very similar to each other, having a rate of about 4.5 scans/cycle. This is equivalent to a frequency of about 20 cycles/sec.

This approach was repeated using measured data that had been smoothed. The results were unchanged.

It was assumed that points 90-130 were representative of the periodic noise and that in the other regions the periodicity was less apparent due to the gaussian noise or our approximations in smoothing or fitting the measured data.

To find a representative value for the entire scan the bias curves for each of the several points (90-130) on the scan were averaged. The periodic effect of the noise was then removed by subtracting the bias value derived for each

scan from every point on that scan. Because we chose not to assume either a positive or a negative noise addition and because a constant value, different for each curve, (the smallest amplitude) was subtracted, no zero reference exists. The periodic noise was therefore removed to within an additive constant which was determined through the scaling process.

The following charts are representative of the periodic curves discussed above.

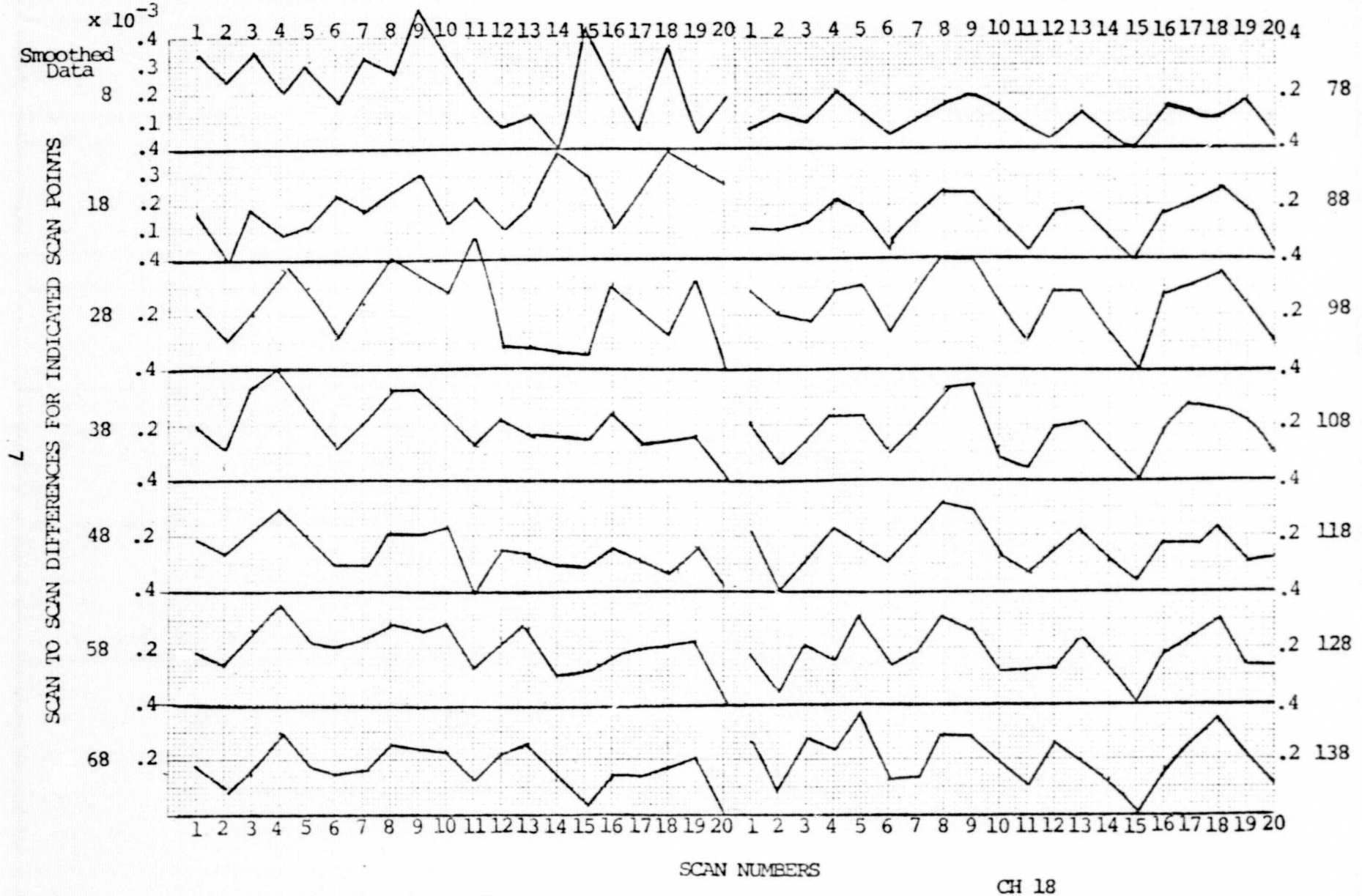

FIGURE 1.A

APPENDIX B

SCALING & CALIBRATION

A. Overlap Calculations

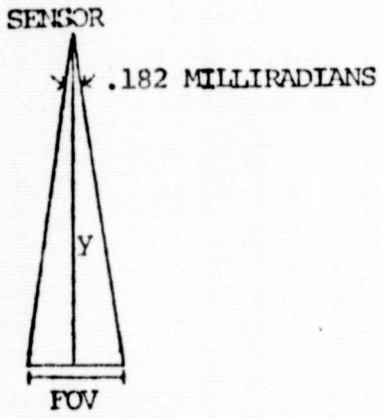

FIGURE B.1

The S192 field of view (FOV) is the product of solid angle subtended by the sensor and the distance to the scene. In the case of the earth Y = 435 Km; for the limb of the earth Y $\tilde{=}$ 2400 Km.

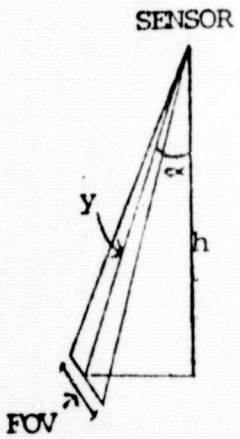

FIGURE B.2

To calculate the overlap from pixel to pixel we wish to unfold the cone generated by the S192 sensor. As shown in figure B.2 the optical line of sight rotates about an axis extended an angle α from the axis, where $\alpha = 5^{O}32'$. The circumference of the circle generated by rotating the field of view around the axis is

$$c = 2\pi x$$

where $x = h \tan \alpha$. The scan line encompasses $116^{O}15'$ of the circle. The length, s, of the scan line is then

$$s = \frac{116.25^{O}}{360^{O}} C$$

$$= \frac{116.25}{360} 2\pi x$$

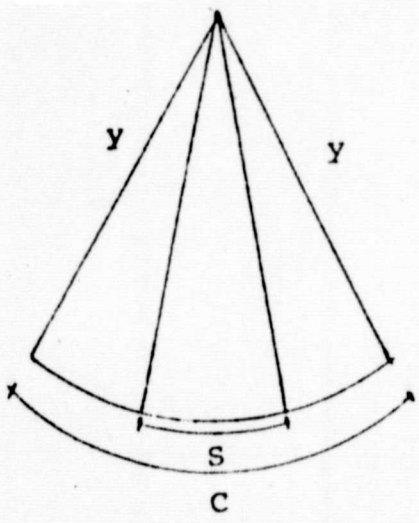

FIGURE B.3

The generated cone can be unfolded into a two-dimensional figure as shown in figure B.3. Let θ be the angle that arc c subtends and let β be the angle that s subtends:

$$\theta = \frac{c}{y}$$

$$\beta = s/y$$

$$= \frac{116.25}{360} 2\pi \frac{x}{y}$$

$$= \frac{116.25}{360} 2\pi \sin \alpha$$

$$= .19563 \text{ radians}$$

Note that

$$.000182 \frac{\text{radians}}{\text{pixel}} 1240 \frac{\text{pixels}}{\text{scan}} = .22568 \text{ radians/scan}$$

The difference between .22568 radians/per scan and .19563 radians per scan is the composite overlap for the scan expressed in angles. Since there are 1239 overlaps/scan, overlap per pixel is

$$\frac{.22568 - .19563}{1239} = .0242528 \text{ milliradians}$$

Expressed in meters this is

$$.0242528 \text{ milliradians} \times 2400 \text{ km} = 58.2 \text{ meters}$$

This overlap on the earth would be

$$(.0242528)\ (435) = 10.5 \text{ meters}$$

This overlap compares with the overlap of 6.65 meters reported in the NASA documentation.

APPENDIX B

SCALING AND CALIBRATION

B. Change of Altitude Increment

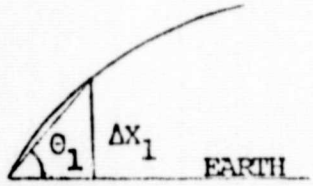

FIGURE B.4

The altitude increment is dependent on the position of scan relative to the earth. This can be represented as the angle of intersection, θ_1, between the scan arc and the earth's surface. All altitude increments Δx_i can be determined from the θ_1 and known characteristics of the scan arc.

The arc between two adjacent points subtends an angle of $\alpha = 116.25^{\circ}/1239$ pts. The arc between the first point and any point i subtends an angle of $\beta_i = \frac{(i-1)}{1239} (116.25)^{\circ}$.

We wish to express θ_i in terms of θ_1 and β_i.

From figure B.5 it is shown that $\theta_i = \theta_1 - \beta_i$

$$= \theta_1 - \frac{(I - 1)}{1239} (116.25^{\circ})$$

Therefore

$$\Delta x_i = s \sin \theta_i$$

where s is the center to center spacing between points.

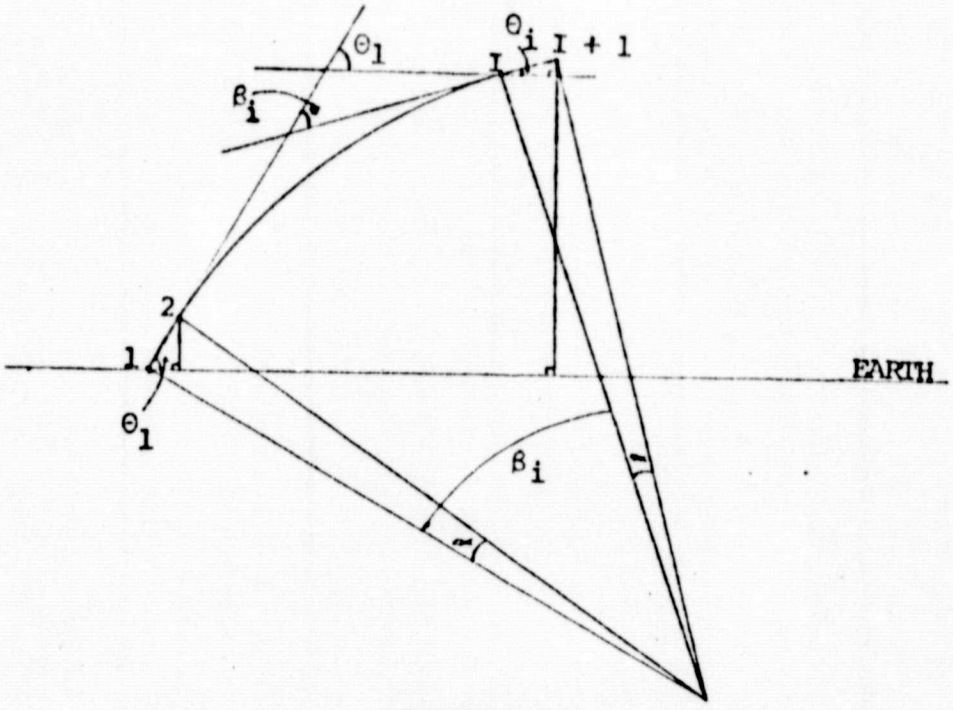

FIGURE B.5

APPENDIX B

SCALING AND CALIBRATION

C. Calibration

The multiplicative scale factor, a, needed to calibrate the recorded intensity is obtained by fitting the measured curve against a model. The model was derived from the attenuation coefficients reported by Elterman in 1968 ("UV, Visible, and IR Attenuation for Altitudes to 50 km, 1968", Air Force Cambridge Research Laboratories). Details of the derivation of the model is discussed in Appendix C.

As discussed in Appendix A, the removal of the periodic noise also left an undetermined additive constant, b, on the intensity scale. These two constants were obtained by solving an overdetermined set of linear equations to find a least squares fit of the measured data to the model.

Thus,

$$y_i = a\, x_i + b \qquad i = 1, \ldots, 30$$

where y_i = model intensity

x_i = measured intensity

The thirty points were selected from along the scan line by incrementing every 20 points from points 1-81 and every 2 points from points 100-148. The emphasis on the upper altitudes was because the aerosol contribution approaches insignificance, therefore deviations of the data from the model would also approach insignificance, assuming a constant Rayleigh contribution. The lower altitudes must be included to some degree, however, to maintain the same general curve structure.

APPENDIX B

SCALING AND CALIBRATION

D. Skybet Pointing Accuracy

Forcing the measured data curve to fit a model curve was necessary partly because of the inaccuracies in the housekeeping data recorded on the Skybet tape. From NASA document PHO-TR 524 Rev A, page B-1, location of the intersection point of the sensor pointing vector and the earth model ellipsoid is accurate to within a 3.0 n.mi. tolerance. Extending this tolerance from an altitude of 435 Km on the earth to 2400 Km on the limb gives a possible error of

$$x = 3 \text{ n.mi.} \frac{1.85 \text{ Km}}{\text{n.mi.}} \frac{2400 \text{ Km}}{435 \text{ Km}}$$

$$\doteq 30.6 \text{ Km}$$

For our purposes it is important to locate the field of view to within a few kilometers, hence the need to scale the data by what one might reasonably expect to find as a function of altitude.

Several attempts were made to scale using the Skybet information but all were unsatisfactory. Not only was the location of the field of view unknown, but also the spatial increment between data points was unknown; as follows:

Let $\overrightarrow{SPU'}$ be the sensor pointing vector in ECT', a coordinate system very close to ECT, and let $\overrightarrow{SPU}$ be the sensor pointing vector in ECT. $\overrightarrow{SC}$ is the spacecraft vector in ECT (Earth Centered True).

$$A \cdot \overrightarrow{SPU'} = \overrightarrow{SPU}$$

where A is a 3 x 3 matrix which accounts for the error in $\overrightarrow{SPU'}$.

If θ is the angle between the spacecraft vector and the sensor pointing vector emanating from the spacecraft,

$$\cos\theta = \frac{\overrightarrow{SPU} \cdot -\overrightarrow{SC}}{|\overrightarrow{SPU}| \cdot |\overrightarrow{SC}|} = \frac{(A \cdot \overrightarrow{SPU}') \cdot -\overrightarrow{SC}}{|A \cdot \overrightarrow{SPU}'| \; |\overrightarrow{SC}|}$$

h = spacecraft altitude

R = radius of earth

x = altitude of pointing vector

$$= (R + h) \sin\theta - R$$

$$x = (R + h) \sin\left[\cos^{-1}\left(\frac{(A \cdot \overrightarrow{SPU}') \cdot -\overrightarrow{SC}}{|A \cdot \overrightarrow{SPU}'| \; |\overrightarrow{SC}|}\right)\right]$$

$$x_2 - x_1 = (R + h) \sin\left[\cos^{-1}\left(\frac{(A - \overrightarrow{SPU}'_1) \cdot -\overrightarrow{SC}}{|A \cdot \overrightarrow{SPU}'_1| \; |\overrightarrow{SC}|}\right)\right]$$

$$- \sin\left[\cos^{-1}\left(\frac{(A \cdot \overrightarrow{SPU}'_2) \cdot -\overrightarrow{SC}}{|A \cdot \overrightarrow{SPU}'_2| \; |\overrightarrow{SC}|}\right)\right]$$

which shows that the difference in altitude is not a simple linear relationship with the difference in sensor pointing vectors. The unknown transformation matrix A containing pointing errors cannot be removed. Calculations show that constructed A matrices with 1% error on the diagonal and very small off-diagonal errors will, as expected, produce the 30 km error tolerance predicted with a non-constant change in altitude between adjacent data points. Skybet data were for this reason not used for purposes of field-of-view location.